Excited-state absorption in erbium-doped silica fiber with simultaneous excitation at 977 and 1531 nm

Yu. O. Barmenkov,[1,a)] A. V. Kir'yanov,[1] A. D. Guzmán-Chávez,[1] José-Luis Cruz,[2] and Miguel V. Andrés[2]
[1]*Centro de Investigaciones en Óptica, Loma del Bosque 115, Col. Lomas del Campestre, 37150 León, Guanajuato, Mexico*
[2]*Departamento de Física Aplicada, ICMUV, Universidad de Valencia, Dr. Moliner 50, E46100 Burjassot (Valencia), Spain*

(Received 6 June 2009; accepted 22 September 2009; published online 26 October 2009)

We report a study of the excited-state absorption (ESA) in erbium-doped silica fiber (EDF) pumped at 977 nm, when the fiber is simultaneously excited by signal radiation at 1531 nm. We show, both experimentally and theoretically, that ESA efficiency at 977 nm gets strongly enhanced only in the presence of signal power. Experimentally, this conclusion is supported through the detection of upconversion emission, a "fingerprint" of the ESA process, and through the measurements of the EDF nonlinear transmission coefficient for the pump wavelength, which is sensitive to the ESA value. It is shown that the experimental data are precisely modeled with an advanced five-level Er^{3+} model developed for the EDF. © *2009 American Institute of Physics*. [doi:10.1063/1.3248369]

I. INTRODUCTION

One of the contemporary telecom trends relates to engineering with erbium (Er^{3+})-doped fiber lasers (EDFL) and amplifiers (EDFA), reliable and widely applicable fiber devices for the main telecom transmission window (~1.5–1.6 μm).[1–5] However, EDFL/EDFA are not free from certain disadvantages. One can point out their relatively low efficiency comparing to ytterbium (Yb^{3+})-doped fiber lasers and amplifiers, and the tendency to possess a relatively high-level noise or even self-pulsing.[6–10] One of the self-pulsing sources in EDFL, as it stems from a series of previous works,[11–17] is the presence of excited-state absorption (ESA) in Er^{3+}. ESA is immanent to the Er^{3+} system while an Er^{3+}-doped silica fiber (EDF) is pumped through its ground-state absorption (GSA) bands, centered at ~977 and ~1531 nm.[11,12] ESA appears immediately after populating the excited states $^4I_{13/2}$ ("2") and $^4I_{13/2}$ ("3") of Er^{3+} through the GSA transitions "1"→"2" (~1480–1590 nm: $^4I_{15/2} \rightarrow {}^4I_{13/2}$) and "1"→"3" (~977 nm: $^4I_{15/2} \rightarrow {}^4I_{11/2}$) (see Fig. 1). The correspondent ESA processes in EDF are, respectively, $^4I_{13/2} \rightarrow {}^4I_{9/2}$ ("2"→"4") and $^4I_{11/2} \rightarrow {}^4F_{7/2}$ ("3"→"5").

In spite of the necessity to clarify the impact of the ESA processes on EDFL/EDFA operation, very few studies have been so far reported on the theme. Meanwhile, the definitions of the ESA parameters and their values differ in the literature.[12,16] In our previous work,[16] we considered the spectral features of the ESA process "2"→"4" within the wavelength interval 1.48–1.59 μm. In that paper we reported the value of the ESA parameter $\varepsilon_s = \sigma_{24}/\sigma_{12}$ that corresponds to the transition $^4I_{13/2} \rightarrow {}^4I_{9/2}$ (here and through the text remainder, σ_{ij} are the cross-sections for the transitions $i \rightarrow j$) and demonstrated that upconversion emission (UCE), attributing $^4I_{11/2} \rightarrow {}^4I_{15/2}$ transition, provides useful information on the ESA process "2"→"4".

In the present work, we provide the reader with further results on the ESA physics in EDF. We study, both experimentally and theoretically, another ESA process, $^4I_{11/2} \rightarrow {}^4F_{7/2}$ ("3"→"5" on Fig. 1), which takes place when EDF is excited simultaneously at the two GSA wavelengths λ_p ~977 nm and λ_s ~1531 nm. An important aspect is that such a situation is normally encountered in a diode-pumped (λ_p ~975–980 nm) EDFL or EDFA. Since the signal radiation at the induced transition $^4I_{15/2} \rightarrow {}^4I_{13/2}$ ("2"→"1") is intrinsically present in EDFL and EDFA, the knowledge of the ESA value at the pump wavelength λ_p in the presence of radiation at the signal wavelength λ_s is desirable. Our results demonstrate that ESA at λ_p may play a notable role as a strong pump loss factor in EDF. The data for the ESA process (at λ_p) in the presence of signal radiation (at λ_s) seem to be important indeed because the presence of signal radiation in EDF results in an increased populating of state $^4I_{11/2}$, from where ESA $^4I_{11/2} \rightarrow {}^4F_{7/2}$ ("3"→"5") starts. On the con-

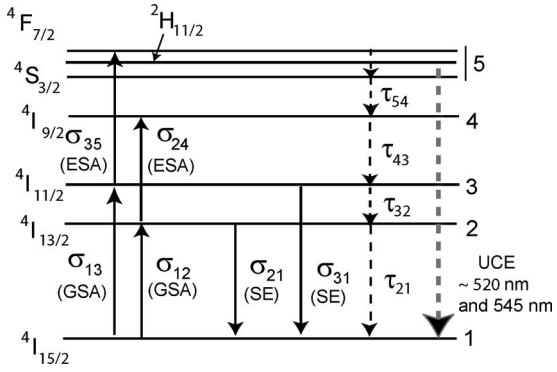

FIG. 1. Er^{3+} five-level scheme used for modeling. Levels $^4F_{7/2}$, $^2H_{11/2}$, and $^4S_{3/2}$ are regarded as an effective level "5." σ_{ij} and τ_{ij} are, respectively, cross-sections and decay times for the transitions between the levels i and j.

a)Electronic mail: yuri@cio.mx.

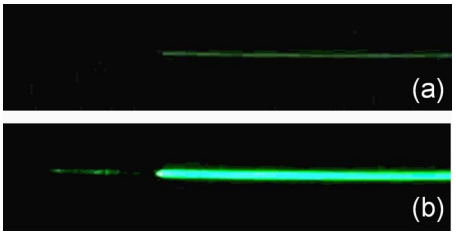

FIG. 2. (Color online) Photographs of ~520/~545 nm UCE obtained from the EDF lateral surface at in-core excitation (a) only at λ_p=977 nm (P_p=260 mW) and (b) simultaneously at λ_p=977 nm and λ_s=1531 nm (P_p=P_s=260 mW).

trary, without the presence of signal wave in the fiber, almost all ions will be in the upper laser level $^4I_{13/2}$, which leads to a low pump absorption. Thus, the signal at 1531 nm switches on the ESA process at λ_p and, thereafter, it increases the number of Er^{3+} ions in the ground state, leading to an increase in the pump absorption. Consequently, there will be a non-negligible population of ions on the level $^4I_{11/2}$ and so a more effective ESA process at the pump wavelength.

II. EXPERIMENTAL RESULTS

One of our objectives is the determination of the ESA parameter at the pump wavelength (λ_p~977 nm), $\varepsilon_p = \sigma_{35}/\sigma_{13}$, in the presence of signal (amplified) emission at the wavelength λ_s~1531 nm (σ_{13} and σ_{35} are the GSA and ESA cross-sections, see Fig. 1). In our experiments, we measured (i) the nonlinear transmission coefficient T_p at λ_p and (ii) the UCE power P_{UCE} (green spontaneous emission peaked at ~520 and ~545 nm, the transitions $^2H_{11/2} \rightarrow {}^4I_{15/2}$ and $^4S_{3/2} \rightarrow {}^4I_{15/2}$), both for a fixed pump power (P_p) and variable signal power (P_s).

In experiments, we used a low-doped silica EDF (Thorlabs M5–980–125, ~300 ppm of Er^{3+} concentration, Al–Ge-silicate host composition) to ensure a negligible contribution from Auger upconversion, the effect observed in heavy-doped EDF owing to the presence of Er^{3+}–Er^{3+} pairs.[11,17,18] So, the results discussed below are almost free from the pairs' effect, so the nonlinearity occurring in the EDF transmission coefficient and UCE stem both solely from ESA.

The first experiment was focused on the demonstration of the presence of ESA in the EDF, when it is pumped simultaneously at λ_p=977 nm (through $^4I_{15/2} \rightarrow {}^4I_{11/2}$ transition) and at λ_s=1531 nm (through $^4I_{15/2} \rightarrow {}^4I_{13/2}$ transition). It was aimed on the observation of UCE (transitions $^2H_{11/2} \rightarrow {}^4I_{15/2}$ and $^4S_{3/2} \rightarrow {}^4I_{15/2}$ "5" → "3", see Fig. 1), which follows ESA at λ_p.

Experimentally, an EDF piece was pumped, using a wavelength division multiplexer (WDM) supporting up to 1 W of optical power, by the pump and signal beams from the same fiber side. These beams were delivered, correspondingly, from a standard fibered semiconductor laser (λ_p=977 nm) and another semiconductor laser with wavelength λ_s=1531 nm, followed by an EDFA.

Figure 2 shows two photographs of lateral emission from the EDF when the fiber was pumped, respectively, (i) only at wavelength λ_p [Fig. 2(a)] and (ii) simultaneously at wavelengths λ_p and λ_s [Fig. 2(b)]; the incidence pump and signal

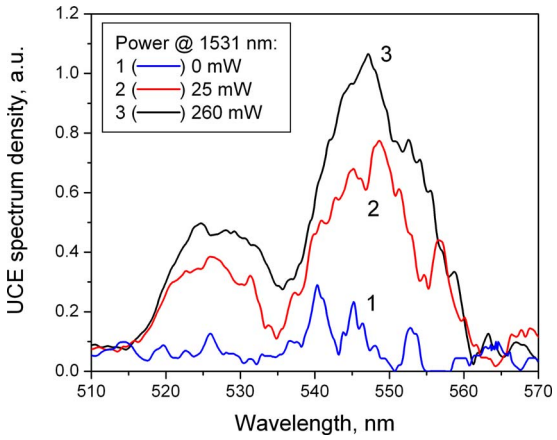

FIG. 3. (Color online) Frontal UCE spectra recorded from a 5 cm EDF piece at in-core excitation at pump wavelength λ_p=977 nm (P_p=260 mW) and variable (P_s=0, 25, and 260 mW) signal power (λ_s=1531 nm).

powers were P_p=P_s=260 mW. One can readily see from Fig. 2 remarkably bright UCE (in the green spectral range, ~520–560 nm) when the EDF is pumped at both wavelengths λ_p and λ_s. Notice that UCE was vastly weak when the fiber was pumped at only wavelength λ_p.

The EDF UCE spectra, obtained for a 5 cm EDF piece using an optical spectrum analyzer, are shown in Fig. 3. The spectra were recorded for three different signal powers (0, 25, and 260 mW) and fixed pump power (260 mW). From Fig. 3, one can see that (i) even low-power (25 mW) signal radiation tremendously enhances UCE (compare curves 1 and 2) and (ii) if it is further increased up to P_s=260 mW, the UCE power growth becomes slower, demonstrating a saturating behavior (compare curves 2 and 3). So the conclusion can be made from Figs. 2 and 3 that stronger UCE is the appearance of noticeably strong ESA in the EDF. Another conclusion is that although the ESA process at λ_p=977 nm is the origin of UCE (see Fig. 1), its brightness is drastically increased upon the assistance of signal wave radiation at wavelength λ_s=1531 nm.

Figure 4 shows the dependence of green UCE signal

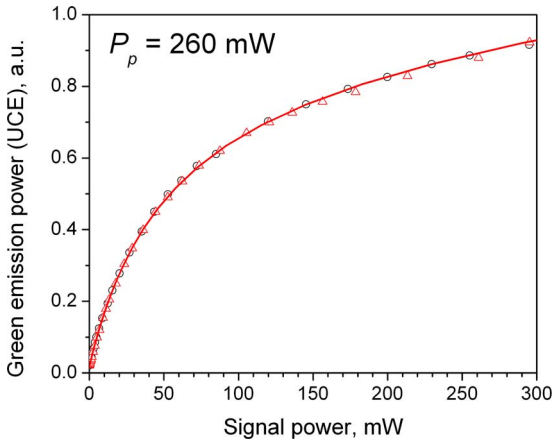

FIG. 4. (Color online) Dependence of UCE power on signal power. Circles and triangles correspond to different experimental series obtained at the same conditions; the plain curve is the theoretical fit. In each case, pump power is fixed at P_p=260 mW and signal power P_s is varied from 0 to ~300 mW.

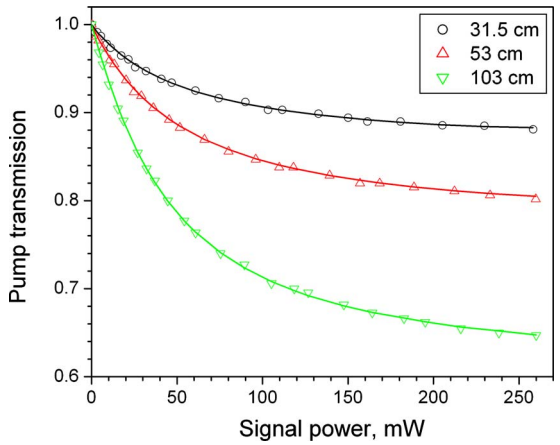

FIG. 5. (Color online) Experimental (symbols) and theoretical (plain curves) dependences of pump wave (λ_p=977 nm) transmission coefficient on signal wave (λ_s=1531 nm) power; the data are obtained for three different EDF lengths (see inset). Theoretical curves are the best fits to the experimental data (ε_p=0.95 and ξ_p=1.08).

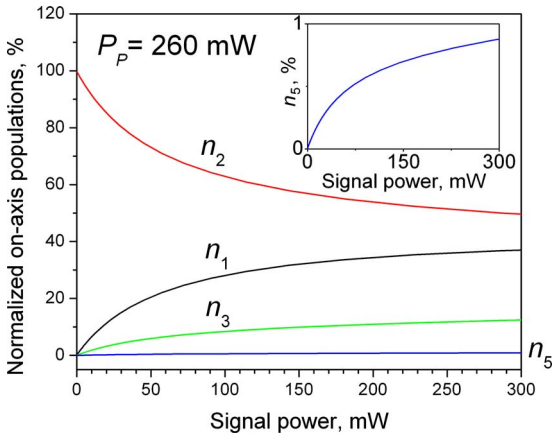

FIG. 6. (Color online) Calculated dependences of populations of Er^{3+} levels on signal power at pump power fixed at 260 mW. The ESA and SE parameters for the pump and signal waves are taken as ε_p=0.95; ξ_p=1.08 and ε_s=0.17; ξ_s=1.08.

detected from the EDF on powers of pump and signal radiations launched into the fiber (in this case, again, the pump power was kept fixed, P_p=260 mW, and the signal power was varied, P_s=0–290 mW). Experimentally, lateral UCE power $P_{\mathrm{UCE}}(P_s)$ was measured using a photomultiplier with a cesium cathode from a short section (~1 mm) of the EDF near its splice with the WDM.

It is seen that UCE behavior has the details already discussed. At very low signal power, UCE power is extremely weak, while upon its increase, UCE power first strongly grows and then gets saturated. The experimental dependence shown in Fig. 4 by symbols (circles and triangles) is fitted by a plain curve, which represents the modeling results discussed in Sec. III.

Another series of experiments, showing the relevance of the ESA process at λ_p=977 nm, was performed through the measurement of the EDF transmission coefficient at λ_p as a nonlinear dependence of signal power.

The experiments included the direct measurements of the signal and pump powers at the EDF input and output at fixed input pump power ($P_{p\ \mathrm{in}}$=260 mW) and output power $P_{p\ \mathrm{out}}$ measured for each value of signal power P_s(P_s=0–260 mW). From the experimental data we obtained the EDF transmission coefficient as a dependence of input signal power $T_p(P_s)=P_{p\ \mathrm{out}}/P_{p\ \mathrm{in}}$. To decrease the role of unwanted amplified spontaneous emission (ASE), we used in the experiments short pieces of the EDF (≤1 m), for making the ASE contribution negligible.

The examples of the dependences $T_p(P_s)$ obtained for different EDF lengths are shown in Fig. 5. The shape of the curves and the divergence between them appear as a result of superposition of the processes involved at the EDF excitation, i.e., of the GSA, ESA, and stimulated emission (SE) transitions at the wavelengths λ_p and λ_s and also of the radiative and phonon-assisted (nonradiative) decays within the Er^{3+} ions system (see Fig. 1). A theory developed to model the experimental data plotted in Figs. 4 and 5 is discussed in the next section.

III. MODELING AND DICSUSSION

We consider an effective five-level Er^{3+} system (Fig. 1) for the EDF upon excitation at wavelengths λ_p and λ_s. First, we derive a model for the dependence of UCE power and the nonlinear transmission coefficient on signal power (see Figs. 4 and 5), and then we discuss the results.

Simultaneous excitation of EDF at the pump and signal wavelengths through the GSA transitions ("1" → "3": ${}^4I_{15/2} \rightarrow {}^4I_{11/2}$ and "1" → "2": ${}^4I_{15/2} \rightarrow {}^4I_{13/2}$) results in a partial but noticeable (comparing to the case of excitation at only λ_p) populating of state "3" (${}^4I_{11/2}$), which allows, thereafter, the populating of short-living state ${}^4F_{7/2}$ through ESA transition "3" → "5": ${}^4I_{11/2} \rightarrow {}^4F_{7/2}$. At the two-wavelength excitation, the SE transitions at wavelengths λ_p and λ_s from the excited states ${}^4I_{11/2}$ and ${}^4I_{13/2}$ to the ground state (${}^4I_{15/2}$), as well as the ESA process at λ_s ("2" → "4": ${}^4I_{13/2} \rightarrow {}^4I_{9/2}$) are of importance. The nonradiative phonon-assisted decays ($\tau_{i,i-1}$, i=1–5) should be accounted for to complete the model. To simplify the balance equations and to make them physically clear, we deal further with the ESA parameters $\varepsilon_p=\sigma_{35}/\sigma_{13}$ and $\varepsilon_s=\sigma_{24}/\sigma_{12}$ and the parameters that characterize the SE to GSA cross-sections' ratios at λ_p and λ_s ($\xi_p=\sigma_{31}/\sigma_{13}$ and $\xi_s=\sigma_{21}/\sigma_{12}$). These equations, which address the Er^{3+} ion system functioning at the two-wavelength (λ_p and λ_s) excitation, at the steady-state are as follows:

$$\frac{\sigma_{12}I_s}{h\nu_s}N_1 - \frac{\sigma_{21}I_s}{h\nu_s}N_2 - \frac{\sigma_{24}I_s}{h\nu_s}N_2 - \frac{N_2}{\tau_{21}} + \frac{N_3}{\tau_{32}} = 0, \tag{1a}$$

$$\frac{\sigma_{13}I_p}{h\nu_p}N_1 - \frac{\sigma_{31}I_p}{h\nu_p}N_3 - \frac{N_3}{\tau_{32}} - \frac{\sigma_{35}I_p}{h\nu_p}N_3 + \frac{N_4}{\tau_{43}} = 0, \tag{1b}$$

$$\frac{\sigma_{24}I_s}{h\nu_s}N_2 - \frac{N_4}{\tau_{43}} + \frac{N_5}{\tau_{54}} = 0, \tag{1c}$$

$$\frac{\sigma_{35}I_p}{h\nu_p}N_3 - \frac{N_5}{\tau_{54}} = 0, \tag{1d}$$

TABLE I. Parameters used in modeling.

Parameter	Value	Units
Low-signal absorption at 1531 nm[a]	$\alpha_{s0}=0.016$	cm^{-1}
Low-signal absorption at 977 nm[a]	$\alpha_{p0}=0.012$	cm^{-1}
Fiber numerical aperture[b]	$NA=0.24$	
Cutoff wavelength[b]	$\lambda_c=940$	nm
ESA parameter at 1531 nm[c]	$\varepsilon_s=0.17$	
SE/GSA cross-section ratio at 1531 nm[c]	$\xi_s=1.08$	
Saturation power at 1531 nm[a]	$P_{ssat}=0.287$	mW
Saturation power at 977 nm[a]	$P_{psat}=0.350$	mW
Relaxation time for $^4I_{13/2}\rightarrow{}^4I_{15/2}$ transition[a]	$\tau_{21}=10$	ms
Relaxation time for $^4I_{11/2}\rightarrow{}^4I_{13/2}$ transition[d]	$\tau_{32}=5.2$	μs
Relaxation time for $^4I_{9/2}\rightarrow{}^4I_{11/2}$ transition[e]	$\tau_{43}=5$	ns
Relaxation time for $(^4F_{7/2}/{}^2H_{11/2}/{}^4S_{3/2})\rightarrow{}^4I_{9/2}$ transition[f]	$\tau_{54}=1$	μs

[a]Experimental data.
[b]Supplier data.
[c]Data from Ref. 16.
[d]Experimental data (compare with Refs. 17 and 19).
[e]Data from Ref. 19.
[f]Data from Refs. 14 and 21–23.

$$N_1+N_2+N_3+N_4+N_5=N_0, \tag{1e}$$

where h is the Plank constant, ν_p and ν_s are the frequencies of the pump and signal waves, I_s and I_p are the pump and signal waves' intensities, N_i are the populations of the correspondent Er^{3+} levels ($i=1-5$), and N_0 is the Er^{3+} dopants concentration in the EDF core. To solve the system of Eqs. (1a) and (1e), we introduce the notations for the normalized populations of the Er^{3+} levels: $n_i=N_i/N_0$. (Notice here that the population of the fourth level ($^4I_{9/2}$) is zeroed, as it decays with the time constant $\tau_{43}=5$ ns, i.e., much rapidly than any other one, see Table I). Meanwhile, despite the decay of the fifth level ($^4F_{7/2}/{}^2H_{11/2}/{}^4S_{3/2}$) is as well relatively short, its population cannot be neglected as a necessary parameter for modeling UCE at ~525–540 nm, see below). The solution for the set of Eqs. (1a)–(1e) can be obtained as follows:

$$n_1=\begin{vmatrix} c_1 & a_{12} \\ c_2 & a_{22} \end{vmatrix} \Big/ \begin{vmatrix} a_{11} & a_{12} \\ a_{21} & a_{22} \end{vmatrix}, \tag{2a}$$

$$n_2=\begin{vmatrix} a_{11} & c_1 \\ a_{21} & c_2 \end{vmatrix} \Big/ \begin{vmatrix} a_{11} & a_{12} \\ a_{21} & a_{22} \end{vmatrix}, \tag{2b}$$

$$n_3=\frac{1-n_1-n_2}{1+\varepsilon_p\gamma_2 s_p}, \tag{2c}$$

$$n_5=\varepsilon_p\gamma_2 s_p n_3, \tag{2d}$$

where

$$a_{11}=(1+\varepsilon_p\gamma_2 s_p)s_s-\gamma_1, \tag{3a}$$

$$a_{12}=-[1+\gamma_1+(\xi_s+\varepsilon_s)s_s+\varepsilon_p\gamma_2 s_p+(\xi_s+\varepsilon_s)\varepsilon_p\gamma_2 s_s s_p], \tag{3b}$$

$$a_{21}=\gamma_1+(1+\xi_p)s_p+\varepsilon_p\gamma_2 s_p^2, \tag{3c}$$

$$a_{22}=\gamma_1+\xi_p s_p+(1+\varepsilon_p\gamma_2 s_p)\varepsilon_s s_s, \tag{3d}$$

$$c_1=-\gamma_1, \tag{3e}$$

$$c_2=\gamma_1+\xi_p s_p, \tag{3f}$$

with values ε_p, ε_s, ξ_p, and ξ_s being defined above. In Eqs. (2a), (2d), and (3a)–(3f) we use, to simplify the notation, the following parameters, which are the products of the already introduced quantities: (i) a couple of "relative time parameters," $\gamma_1=\tau_{21}/\tau_{32}$ and $\gamma_2=\tau_{53}/\tau_{21}$, and (ii) another couple of "saturation parameters" for the signal and pump waves, $s_s=I_s/I_{ssat}$ and $s_p=I_p/I_{psat}$, where the saturation intensities at wavelengths λ_p and λ_s are defined, respectively, as $I_{ssat}=h\nu_s/\sigma_{12}\tau_{21}$ and $I_{psat}=h\nu_p/\sigma_{13}\tau_{21}$.

(1) To model the dependences of UCE power on signal power $P_{UCE}(P_s)$ (see Fig. 4), one can use Eq. (2d) for population n_5 of level "5," from where UCE in the visible originates. By the way, notice that n_5 relates to the ESA process "3" → "5" and directly depends on ε_p [see Eqs. (2c) and (2d)]. As spontaneous UCE power P_{UCE} is proportional to n_5, its calculation, as a dependence of I_s (or P_s), is sufficient to find the sought law. In order to get a true dependence, one needs to make the averaging of the n_5 value over the EDF core, remembering that the intensities of the pump and signal waves are distributed within the fiber according to the Gaussian law, $s_{p,s}(r)=s_{p0,s0}\exp[-2(r/w_{p,s})^2]$, where $w_{p,s}$ are the pump and signal beams' radii. Taking into account the latter, the averaged value for n_5 takes the form

$$\bar{n}_5=\frac{\varepsilon_p\gamma_2}{a^2}\int_0^a \frac{1-n_1(r)-n_2(r)}{1+\varepsilon_p\gamma_2 s_p(r)} s_p(r)2rdr, \tag{4}$$

where a is the EDF core radius. Now, the experimental dependence shown in Fig. 4 can be directly modeled, implying $P_{UCE}\propto\bar{n}_5$, with some proportionality coefficient.

(2) To address the EDF nonlinear transmission coefficient at the pump wavelength as a dependence of signal power $T_p(P_s)$ (for modeling the experimental dependences shown in Fig. 5), the system of Eqs. (1a) and (1e) should be accompanied by a couple of equations for the pump and signal waves propagating through the fiber

$$\frac{dI_p}{dz}=-\sigma_{13}N_1 I_p+\sigma_{31}N_3 I_p-\sigma_{35}N_3 I_p, \tag{5a}$$

$$\frac{dI_s}{dz}=-\sigma_{12}N_1 I_s+\sigma_{21}N_2 I_s-\sigma_{24}N_2 I_s. \tag{5b}$$

Taking again the Gaussian radial distributions for these two waves, one can transform Eqs. (5a) and (5b) to the following form:

$$\frac{dP_p}{dz} = \frac{\alpha_{p0}}{\Gamma_p}\frac{2}{w_p^2}\left\{-\int_0^a n_1(r,z)\exp\left[-2\left(\frac{r}{w_p}\right)^2\right]2rdr + (\xi_p-\varepsilon_p)\int_0^a n_3(r,z)\exp\left[-2\left(\frac{r}{w_p}\right)^2\right]2rdr\right\}P_p, \tag{6a}$$

$$\frac{dP_s}{dz} = \frac{\alpha_{s0}}{\Gamma_s}\frac{2}{w_s^2}\left\{-\int_0^a n_1(r,z)\exp\left[-2\left(\frac{r}{w_s}\right)^2\right]2rdr + (\xi_s-\varepsilon_s)\int_0^a n_2(r,z)\exp\left[-2\left(\frac{r}{w_s}\right)^2\right]2rdr\right\}P_s, \tag{6b}$$

where α_{p0} and α_{s0} are, respectively, the low-signal absorption coefficients at the pump and signal wavelengths λ_p and λ_s, Γ_p and Γ_s are the EDF core/beam overlap factors for these wavelengths, and z is the coordinate along the fiber length. From Eqs. (6a) and (6b), one can find the EDF absorption coefficient for the pump wave α_p and the gain coefficient for the signal wave g_s

$$\alpha_p(z) = \frac{2\alpha_{p0}}{w_p^2\Gamma_p}\int_0^a [n_1(r,z)-(\xi_p-\varepsilon_p)n_3(r,z)] \times\exp\left[-2\left(\frac{r}{w_p}\right)^2\right]2rdr, \tag{7a}$$

$$g_s(z) = \frac{2\alpha_{s0}}{w_s^2\Gamma_s}\int_0^a [(\xi_s-\varepsilon_s)n_2(r,z)-n_1(r,z)] \times\exp\left[-2\left(\frac{r}{w_s}\right)^2\right]2rdr, \tag{7b}$$

and the final equations for the pump and signal waves propagating through the fiber

$$dP_p(z) = -\alpha_p(z)P_p(z)dz, \tag{8a}$$

$$dP_s(z) = g_s(z)P_s(z)dz, \tag{8b}$$

where the radial distributions for the normalized populations $n_1(r)$, $n_2(r)$, and $n_3(r)$ are addressed by Eqs. (2a) and (2c), and the Gaussian radial dependence for $s_{s,p}$ is assumed: $s_{s0,p0}=P_{s,p}/P_{s\text{sat},p\text{sat}}\equiv I_{s,p}(r=0)/I_{s\text{sat},p\text{sat}}$. Knowing pump power $P_{p\ \text{in}}$ at the EDF entrance and calculating its value at the fiber exit, we obtain, using Eqs. (6a), (6b), (7a), (7b), (8a), and (8b), the nonlinear transmission coefficients $T(P_{p\ \text{in}})=P_{p\ \text{out}}/P_{p\ \text{in}}$ (for any signal power P_s), the theoretical counterparts to the experimental dependences $T(P_s)$ (see Fig. 5).

In the modeling, we used the data for the EDF (see Table I). Among these, the parameters measured by ourselves are the saturation powers at the pump and signal wavelengths ($P_{p\text{sat}}=I_{p\text{sat}}\times A_p$ and $P_{s\text{sat}}=I_{s\text{sat}}\times A_s$, where $A_{p,s}=\pi(w_{p,s})^2/2$ are the pump and signal beam areas in the EDF), the relaxation times τ_{21} and τ_{32}, and the low-signal absorption coefficients at the pump and signal wavelengths; other necessary quantities were taken either from the EDF supplier's data or from the literature sources relating to EDFs of a similar type. Notice that we take $\tau_{54}=1$ μs, basing on the results for this decay constant obtained for Er^{3+}-doped silicate, alumino-silicate and germano-silicate glasses (see the references in Table I).

The modeling results are shown in Figs. 4 and 5 by plain curves. To fit the experimental data plotted on these figures, we varied only the two parameters, ε_p and ξ_p, which are the characteristics of the ESA and SE transitions at the wavelength $\lambda_p=977$ nm. Their best fits for a whole set of the experimental data have been obtained as $\varepsilon_p=0.95$ and $\xi_p=1.08$. It is seen that the experimental and theoretical results match fairly well. Notice that the found value for the ESA parameter ($\varepsilon_p=0.95$) is the main result of the present work, which shows that ESA at the pump wavelength is indeed an important extra loss factor in EDF-based lasers and amplifiers. As about the SE parameter ($\xi_p=1.08$), one can see that its value slightly differs from the one normally used ($\xi_p=1$).

In the meantime, it should be noted that the parameters ε_p and ξ_p are wavelength-dependent and their values will therefore deviate from the values reported above for $\lambda_p=977$ nm. The same happens for the parameters ε_s and ξ_s, which will change as a function of the wavelength λ_s.[16] In our experiments, the wavelengths $\lambda_p=977$ and $\lambda_s=1531$ nm were chosen as the representatives common in the practice of EDFL/EDFA.

The modeling results allow one to understand the reasons for using the five-level system for Er^{3+} instead of the traditionally used two-level or three-level ones.[11,20] The main difference that stems from the use of the five-level scheme is a substantial (11%–12%) populating of level "3" (see Fig. 6) from where a pump-ESA starts. This fact, together with an increased populating of the ground state "1" (up to 40%), appears to be a consequence of excitation of the EDF simultaneously at the pump and signal wavelengths. Neglecting of the fifth level population (by zeroing τ_{54}) results in mistakes when one would find the EDF parameters, e.g., ξ_p will differ by 3% when it is modeled using $\tau_{54}=1$ μs and $\tau_{54}=0$. The five-level system allows one to understand also the effect of enforcement of green UCE at the presence of a signal wave in pumped EDF (see Fig. 4), that stems from a nonzero ($\sim$1%) populating of level "5," see Fig. 6.

An insight to the EDF physics concerning the EDF nonlinear transmission coefficient $T_p(P_s)$ can be made by analyzing Fig. 7. In this figure, we reproduce one of the experimental dependences shown in Fig. 5 and plot the theoretical dependences $T_p(P_s)$ generated at the following assumptions: (i) both the parameters ε_p and ξ_p have the values allowing the best fit ($\varepsilon_p=0.95$; $\xi_p=1.08$: black curve 1); (ii) neither ESA nor SE parameter is taken into account ($\varepsilon_p=0$; $\xi_p=0$: blue curve 3); (iii) and (iv) either one of these parameters is taken as "optimal," while the other is zeroed ($\varepsilon_p=0.95$; $\xi_p=0$: green curve 4, and $\varepsilon_p=0$; $\xi_p=1.08$: red curve 5). We also present in Fig. 7 the dependence generated at the assumption that both the parameters ε_p and ξ_p are equal to 1 (black dashed curve 2). Notice that in each of the modeled circumstances, the parameters for the signal wave were kept the same, $\varepsilon_s=0.17$ and $\xi_s=1.08$.[16]

It is seen that the knowledge of ESA parameter ε_p allows the best fit to the experimental data for smaller signal powers

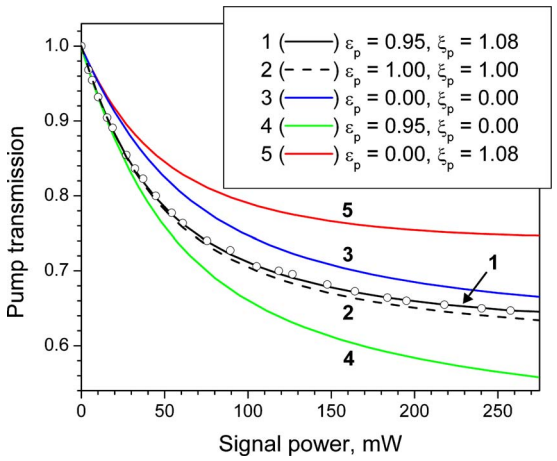

FIG. 7. (Color online) Dispersion of the modeling results when the ESA and SE parameters are varied. The ESA and SE parameters values taken at modeling are indicated in the inset. Circles on the graph repeat the experimental results shown in Fig. 5 for 103 cm EDF.

P_s, whereas the knowledge of the SE parameter ξ_p allows the best fit to the results for higher (saturating) P_s (compare the asymptotic behaviors of the curves at these limits, Fig. 7). Let us also notice the deviation between curves 1 (the best fitting case) and 2 (the case when both parameters ε_p and ξ_p are equal to 1, a tentative assumption). So, the found values $\varepsilon_p=0.95$ and $\xi_p=1.08$ are seen to be the most reliable estimates for modeling EDF-based lasers and amplifiers. Thus, one can reveal a noticeable role of both these parameters, i.e., the ESA parameter for the pump wavelength, ε_p: ${}^4I_{11/2} \rightarrow {}^4F_{7/2}$("3" → "5"), and the SE parameter, also for the pump wavelength, ξ_p: ${}^4I_{11/2} \rightarrow {}^4I_{15/2}$("3" → "1"), as the ones showing "response" of the Er^{3+} system (in our case, the EDF) to simultaneous excitation at the pump and signal wavelengths.

Before we conclude, we remind that the situation described in the present work, i.e., the simultaneous presence of pump and signal radiations at $\lambda_p=977$ nm and $\lambda_s=1531$ nm in EDF, is routinely encountered in the EDFL/EDFA practice. So, the knowledge of realistic values for the ESA and SE parameters, both for the "pump" wavelength (ε_p and ξ_p, the main result of the present research) and for the "signal" wavelength (ε_s and ξ_s, the result of our work[16]) would be of use.

IV. CONCLUSION

In conclusion, we report a study of the ESA process in EDF at the wavelength $\lambda_p=977$ nm, normally used for pumping, when the fiber is simultaneously excited at the signal wavelength $\lambda_s=1531$ nm. The inspected arrangement can be directly related to either EDFL or EDFA (at gain saturation), where always the pump and signal radiations are present in the active fiber. We experimentally show that the ESA process at the pump wavelength becomes considerable yet at moderate signal powers, while it gets enhanced as the signal power grows. On the other hand, in the absence of signal radiation in EDF, ESA at the pump wavelength can be neglected. These observations are validated through the measurement of UCE, the process that follows ESA and which is its "fingerprint." ESA itself is quantitatively addressed through the measurement of the EDF nonlinear transmission coefficient at the pump wavelength. We also present the results of modeling of the ESA processes in EDF, assuming a five-level system of Er^{3+}. The modeling results match whole the set of experimental data, provided the ESA and SE parameters for the pump wavelength are found ($\lambda_p=977$ nm: $\varepsilon_p=0.95$; $\xi_p=1.08$). To the best of our knowledge, the obtained values of parameters ε_p (ESA) and ξ_p (SE) at the pump wavelength λ_p have never been measured or modeled elsewhere.

ACKNOWLEDGMENTS

This work was supported by the Ministerio de Ciencia e Innovación of Spain (Grant Nos. PCI2005-A7-0209 and TEC2008-05490) and by the Generalitat Valenciana (Grant No. PROMETEO/2009/077).

[1] E. Desurvire, *Erbium-Doped Fiber Amplifiers: Principles and Applications* (Wiley, Hoboken, 2002).
[2] *Rare-Earth-Doped Fiber Lasers and Amplifiers*, edited by M. J. F. Digonnet (Dekker, New York, 2001).
[3] Y. Sun, J. L. Zyskind, and A. K. Srivastava, IEEE J. Sel. Top. Quantum Electron. **3**, 991 (1997).
[4] D. Venkitesh and R. Vijaya, J. Appl. Phys. **104**, 053104 (2008).
[5] Q. Mao and J. W. Y. Lit, Appl. Phys. Lett. **82**, 1335 (2003).
[6] E. Rønnekleiv, O. Hadeler, and G. Vienne, Opt. Lett. **24**, 617 (1999).
[7] A. Tikhomirov and S. Foster, J. Lightwave Technol. **25**, 533 (2007).
[8] W. H. Loh and J. P. de Sandro, Opt. Lett. **21**, 1475 (1996).
[9] A. V. Kir'yanov, N. N. Il'ichev, and Yu. O. Barmenkov, Laser Phys. Lett. **1**, 194 (2004).
[10] Yu. O. Barmenkov and A. V. Kir'yanov, Opt. Express **12**, 3171 (2004).
[11] A. V. Kir'yanov, Yu. O. Barmenkov, and N. N. Il'ichev, Opt. Express **13**, 8498 (2005).
[12] J. Nilsson, P. Blixt, B. Jaskorzynska, and J. Babonas, J. Lightwave Technol. **13**, 341 (1995).
[13] M. Bolshtyansky, I. Mandelbaum, and F. Pan, J. Lightwave Technol. **23**, 2796 (2005).
[14] P. A. Krug, M. G. Sceats, G. R. Atkins, S. C. Guy, and S. B. Poole, Opt. Lett. **16**, 1976 (1991).
[15] R. S. Quimby, W. J. Miniscalco, and B. T. Thomson, *Proceedings of the Topical Meeting on Optical Amplifiers and Applications, Technical Digest Series*, Vol. 17 (Optical Society of America, Washington, D.C., 1992), Paper No. WE3, p. 67.
[16] A. D. Guzman-Chavez, Yu. O. Barmenkov, and A. V. Kir'yanov, Appl. Phys. Lett. **92**, 191111 (2008).
[17] R. S. Quimby, W. J. Miniscalco, and B. Thompson, J. Appl. Phys. **76**, 4472 (1994).
[18] F. Sanchez, P. Le Boudec, P.-L. François, and G. Stephan, Phys. Rev. A **48**, 2220 (1993).
[19] A. Bellemare, Prog. Quantum Electron. **27**, 211 (2003).
[20] R. S. Quimby, Appl. Opt. **30**, 2546 (1991).
[21] C. B. Layne, W. H. Lowdermilk, and M. J. Weber, Phys. Rev. B **16**, 10 (1977).
[22] C. B. Layne, W. H. Lowdermilk, and M. J. Weber, IEEE J. Quantum Electron. **11**, 798 (1975).
[23] M. P. Hehlen, N. J. Cockroft, T. R. Gosnell, and A. J. Bruce, Phys. Rev. B **56**, 9302 (1997).